

# Performance of Hybrid-Reinforced T-Beam with Recycled Rubberized Concrete

Tarik S. El-Salakawy<sup>1</sup>, Amr A. Gamal<sup>1</sup>, Mohamed Essam Sayed\*<sup>1</sup>

<sup>1</sup> Department of Civil Engineering, Faculty of Engineering at Shoubra, Benha University, Cairo, Egypt

\* Corresponding Author.

E-mail: tarek.abdelgalil@feng.bu.edu.eg, amr.gamaleldin@feng.bu.edu.eg, Mohamed.esam21@feng.bu.edu.eg

**Abstract :** Fiber-reinforced polymer FRP has turned into a practical stand-by construction material for the substitution of steel bars in reinforced concrete RC structures. However, the brittleness of GFRP reduces the ductility of pure GFRP-RC beams. To increase flexural ductility and retain the high-strength feature of the FRP bars, hybrid reinforcement was proposed to solve this problem. This paper discusses the flexural capacity and ductility of rubberized hybrid reinforced concrete (RHRC) T-beams. The current research aims to assess the flexural strength, ductility, and energy dissipation of RHRC T-beams. Eight full-scale RC simply supported T-beams were subjected to a two-point loading test. Control RC T-beams (BS, BS1) were designed with traditional steel bars. The beam (BRF) was designed using GFRP bars only, and the other five beams (BH, BH1, BRH1, BRH2, and BRH3) were reinforced using hybrid rebars using GFRP and steel reinforcement. The percentage of the GFRP bars to steel bars at the mid-span section and the effect of crumb rubber on the hybrid concrete matrix were the main parameters considered in this study. The structural performance in terms of flexural capacity, ductility, cracking, deformations, and failure mode was evaluated. Based on the test results, the use of steel reinforcement in combination with GFRP reinforcement improved the flexural capacity and serviceability in terms of the number of cracks and energy dissipation, while decreasing ductility compared to steel-reinforced beams.

**Keywords:** GFRP bars; rubberized concrete; hybrid reinforcement; flexural capacity; ductility.

## 1. INTRODUCTION

Reinforced concrete beams reinforced with GFRP bars operate differently from reinforced concrete beams with steel bars. The lower elastic modulus of FRP bars results in a reduction in the flexural stiffness of reinforced concrete beams once cracking occurs, resulting in-severe deformations in service loading conditions. As a result, the serviceability limit state had a significant impact on the design of RC components reinforced with FRP bars [1–5]. Several studies have focused on RC beams reinforced with various types of FRP bars [6–10]. Both tension and compression failure modes are acceptable in controlling the design of sections reinforced with FRP bars for flanged sections [11]. Many researchers compared the results of both conventional and FRP concrete beams tested under flexure

loading; the results confirmed the enhancement of ultimate load capacity and the reduction of deflection as well as the ductility of the tested beams [12, 13, 14, 16, 17, 19 and 20]. A hybrid system incorporating fiber-reinforced polymer (FRP) rebar and fiber-reinforced concrete (FRC) was applied to concrete beams in this study [15]. Hybrid reinforcement between steel and FRP was introduced in several previous studies. The results show that hybrid reinforcement improves ductility rather than using pure FRP reinforcement [21, 22, 23, 26, and 29]. Several previous research studies also focused on recycled aggregate concrete, rubberized concrete, and the high-performance behavior of fiber-reinforced concrete cementitious composites. Other concrete mixes were introduced to improve beam ductility in many previous research studies [24, 25, 27, 28, 30, and 31].

Nomenclature			
FRC	Fiber reinforced concrete	fcu	Cube concrete compressive strength
FRP	Fiber-reinforced polymer	Fc'	Cylindrical concrete compressive
GFRP	Glass fiber-reinforced polymer	Strength	
HGFRP	Hybrid Glass fiber-reinforced polymer	fs	Steel tensile stress
HRFT	Hybrid-reinforced	fy	Yield steel stress
C.R.	Crumb rubber	εs	Tensile steel strain
RC	Reinforced concrete	εcu	Ultimate compressive strain of conc.
HSC	High strength concrete	fu	Ultimate tensile stress
NSC	Normal Strength Concrete	Pcr	Flexural cracking load
As	the area of steel bars	Pu	Ultimate load
Rein.	Reinforcement	Cw	Width of crack
Af	Area of glass fiber bars	Nc	Number of crack
NAC	Normal aggregate concrete	W	Weight
RRC	Rubberized recycled concrete	V	Volume
RHRC	Rubberized hybrid reinforced concrete	f* fe	The design stress in the FRP bars
FRPRC	Fiber-Reinforced Polymer Reinforced	f* fu	The ultimate tensile stress bars in the FRP
SRC	Steel-reinforced concrete	agg.	Aggregate
GFRP-RC	Glass fiber reinforced polymer reinforced concrete	Ec	Modulus of elasticity of concrete
Life cycle cost	LCC	Es	Elastic modulus of steel bars
MNC	Mix Normal Strength Concrete	Ef	Modulus of elasticity for GFRP bars
MRC	Mix Rubberized Concrete	Ck	Crack of the concrete
μu	Ductility index for concrete beams	PP	Peak flexural load
K	Flexural Stiffness	Δu	Maximum deflection at ultimate load
fc'	Compressive strength of concrete (cylinder)	SP	Super-plasticizer
fc	Compressive strength of concrete (cube)	γc	Is the partial safety factor for concrete
ft	Ultimate tensile strength of concrete	γs	Is the partial safety factor for steel
fy	Yield strength of steel rebar	LVDTs	linear variable differential transducers
Pcr	Flexural load at first cracking	Mu	Ultimate limit flexure of the cross sec.
T s	Tension force in steel reinforcement bars	Ed	Energy dissipation
T f	Tension force in GFRP bars	μ	Reinforcement ratio
Py	Thel load at steel rebar yielding		
Δcr	Deflection at first cracking		
Δy	Deflection at yield load		
σ	Concrete compressive stress		

**2-Analytical solution**

The ductility of the reinforcing steel comes from its yielding ability, which also acts as a member failure indicator. This strategy must be rethought in light of FRP reinforcement's non-ductile behavior. As long as strength and serviceability requirements are met, both failure modes; FRP rupture and concrete crushing can be used to guide the design of flexural components reinforced with FRP bars. The members need to have a bigger strength reserve to make up for their lack of ductility. Consequently, the safety margin recommended by this guide against failure is greater than that employed in conventional steel-reinforced concrete design [32].

- The fundamental assumptions necessary to fulfill the concepts of equilibrium and compatibility are:
  1. Strain in the concrete and the FRP reinforcement is proportional to the distance from the neutral axis (that is, a plane section before loading remains plane after loading).
  2. The concrete's maximum usable compressive strain, ε<sub>cu</sub>, is considered 0.003.
  3. The tensile strength of concrete is neglected, and FRP reinforcement resists all the tensile stresses.
  4. The tensile behavior of the FRP reinforcement is linearly elastic until failure.
  5. A perfect bond exists between concrete and FRP reinforcement. [32].

The balanced reinforcement ratio is the ratio in which concrete crushing and FRP rupture happen at the same time. Concrete crushing is assumed to occur if the maximum compressive strain in the concrete reaches 0.003. Rupture of the FRP laminate is assumed to occur if the strain in the FRP reaches its design rupture strain (ε<sub>f</sub> = ε\*<sub>f</sub> u) before the concrete reaches its maximum usable strain.

The reinforcement ratio of FRP reinforcement can be estimated from Eq. (1). The balanced FRP reinforcement ratio can be estimated from Eq. (2) [32].

$$\mu_f = A_f / (b \cdot d) \tag{1}$$

$$\mu_{fb} = 0.85 \beta_1 (f'_c / (f^*_{fu})) \cdot (E_f \cdot \epsilon_{cu} / E_f \cdot \epsilon_{cu} + f^*_{fu}) \tag{2}$$

In most cases, failure of T-sections subjected to bending moments with the flange in compression is governed by the rupture of FRP bars.

**2.1 Tensile Brittle Failure of FRP** (μ<sub>f</sub> ≤ μ<sub>fb</sub>)

Failure can also be governed by the crushing of the concrete in compression. In this case, the strength reduction factors shall be estimated according to the compression-brittle failure of concrete:

**2.2 Transition Zone between Tensile and Compression Failures [32]** (μ<sub>fb</sub> < μ<sub>f</sub> < 1.4 μ<sub>fb</sub>)

$$\gamma_c = 2.75 - 0.75 \mu_f / \mu_{fb} \quad \text{and} \quad \gamma_f = 2.75 - 0.75 \mu_f / \mu_{fb}$$

**2.3 Compression Brittle Failure of Concrete:**

$$(\mu_f \geq 1.4 \mu_{fb})$$

**2.3.1 Case I: The FRP reinforcement ratio is greater than the balanced reinforcement ratio.**

When  $\mu_f > \mu_{fb}$ , the failure of the member is initiated by the crushing of the concrete, and the stress distribution in the concrete can be approximated with the equivalent rectangular stress block [32].

The design stress in the FRP bars,  $f_{fe}^*$  can be estimated using Eq. (3) after considering the environmental reduction factors.  $f_{fe}^* / \gamma_f = ((\beta_1 \cdot d - a) / a) E_f \cdot \epsilon_{cu}$  (3)

**2.3.2 Case II: The FRP reinforcement ratio is smaller than the balanced reinforcement ratio.**

When  $\mu_f < \mu_{fb}$ , the failure of the member is initiated by rupture of the FRP bars in tension, and the equivalent rectangular stress block for the concrete is not applicable because the maximum concrete strain (0.003) may not be attained, and we will use the ultimate tensile stress bars in the FRP  $f_f^* f_u$ .

**2.3.3 The ultimate moment capacity for the flanged SFRC sections:**

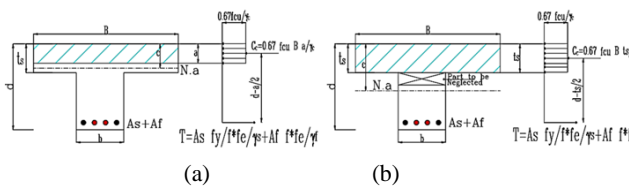


Fig. 1: Analysis of T-beam for the case of the neutral axis in the flange (a) and outside the flange (b)

Assume N.A. is inside the flange, as shown in Fig. 1 (a).

$$T = T_s + T_f \quad (4)$$

$$\blacktriangleright T_s = A_s (f_y / \gamma_s) \quad \text{and} \quad T_f = A_f f^* (f_e / \gamma_f) \quad (5)$$

$$C_c = T_s + T_f \quad (6)$$

$$\blacktriangleright 0.67 f_{cu} B a = A_s (f_y / \gamma_s) + A_f f^* (f_e / \gamma_f) \quad (7)$$

$\blacktriangleright$  get a

$$a = (A_s (f_y / \gamma_s) + A_f f^* (f_e / \gamma_f)) / (0.67 f_{cu} B) \quad (8)$$

$$\text{if } a \leq t_s, \text{ check } \epsilon_s = \epsilon_{cu} (d - c) / c > \epsilon_y \quad (9)$$

$$\blacktriangleright M_u = T_s (d - a/2) + T_f [(d - a/2)] \quad (10)$$

If the N.A. is outside the flange, as shown in Fig. 1 (b)

$$a > t_s$$

$$\blacktriangleright 0.67 f_{cu} \cdot B \cdot t_s = A_s f_y / \gamma_s + A_f f^* f_e / \gamma_f \quad (11)$$

$$M_u = T_s (d - t_s / 2) + T_f [(d - t_s/2)] \quad (12)$$

**3. Experimental Program**

The experimental work of this study was carried out at the Housing and Building National Research Center (HBNRC), Dokki, Egypt, to investigate the performance of a hybrid reinforced T-beam with recycled rubberized concrete in terms of ultimate loads, deflections at mid-span and 1/4 span, crack pattern, and crack propagation.

**3.1. Specimens**

Eight reinforced concrete T-beam specimens containing either steel bars or hybrid reinforcement were investigated and listed in Table 1 and Fig. 2.

Figure 3 shows the reinforcement arrangement for the specimen. The beams were simply supported and subjected to two-point loading, as shown in Fig. 4. A schematic diagram for the eight beams and reinforcement, along with the crump rubber value, is represented in Figs. 2 and 3.

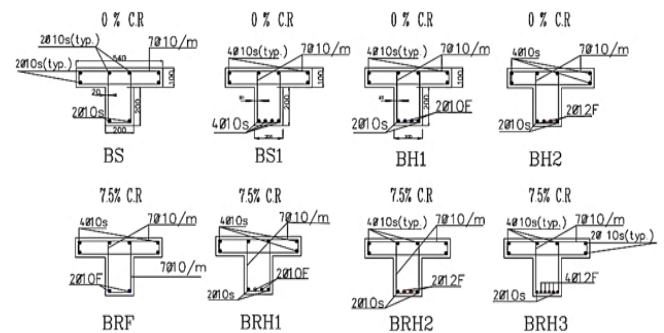


Fig. 2: Tested specimen reinforcement and dimensions (All dimensions are in mm.)

Table 1: Beams-reinforcement, and parameters

No.	Model	% of Crumb Rubber (C.R.)	Bottom RFT	Top RFT	Notes Bottom RFT	Top RFT	A <sub>f</sub> /A <sub>s</sub> (bot.)
1	BS (Control specimen)	0%	2Ø10S	2Ø10	Steel	Steel	0
2	BS1 (Control specimen)	0%	4Ø10S	2Ø10	Steel	Steel	0
3	BH1 (Control specimen)	0%	2Ø10S+2Ø10F	2Ø10	Steel +GFRP	Steel	1
4	BRH1	7.5%	2Ø10S+2Ø10F	2Ø10	Steel +GFRP	Steel	1

5	BRF	7.5%	2Ø10F	2Ø10	GFRP	Steel	-
6	BH2 (Control specimen)	0%	2Ø10S+2φ12F	2Ø10	Steel +GFRP	Steel	1.44
7	BRH2	7.5%	2Ø10S+2φ12F	2Ø10	Steel +GFRP	Steel	1.44
8	BRH3	7.5%	2Ø10S+4φ12F	2Ø10	Steel +GFRP	Steel	2.89

Where RFT is the reinforcement



Fig. 3: Beam longitudinal reinforcement

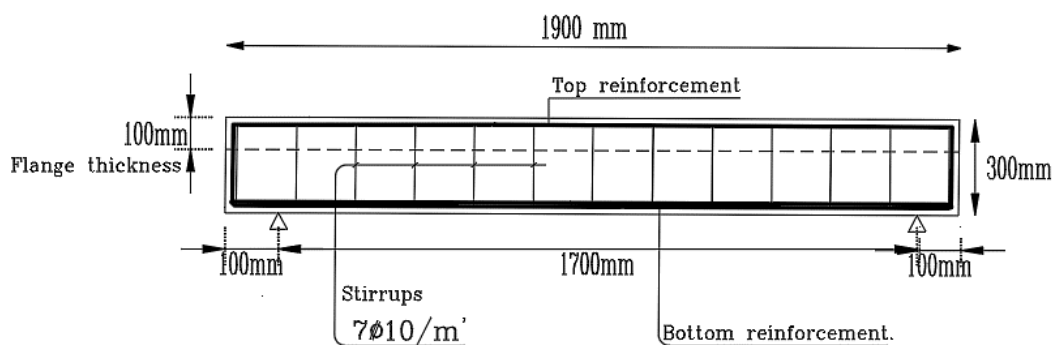


Fig. 4: Beam schematic longitudinal section

Table 2: Mix proportions for concrete mixes

Mix type	C.R. %	Cement	W/C	Water	SP	Fine aggregate (sand)	Coarse aggregate	C.R. W (kg)
		W (kg)		W (kg)		W (kg)	W (kg)	
NC (0% C.R.)	0%	400	0.43	172	5.5	681	1120	0
RC (7.5% C.R.)	7.5%	400	0.43	172	5.5	630	1120	23.35

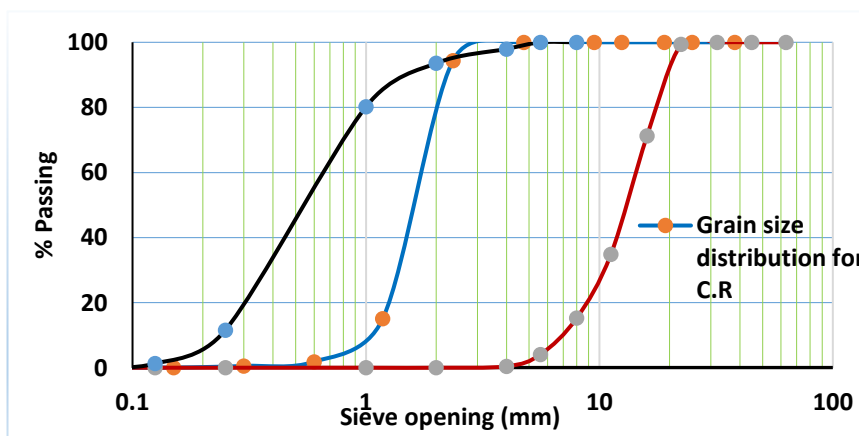


Fig. 5: Fine aggregate, coarse aggregate, and C.R. sieve analysis test

Table 3: Mechanical Properties of Reinforcement

Material	Diameter (mm)	Area (mm)*	Yielding strength (MPa)	Tensile strength (MPa)	Modulus of elasticity (GPa)
GFRP	10	74.70	-	910	40
GFRP	12	87.30	-	989	40
Steel	10	78.50	540	641	190

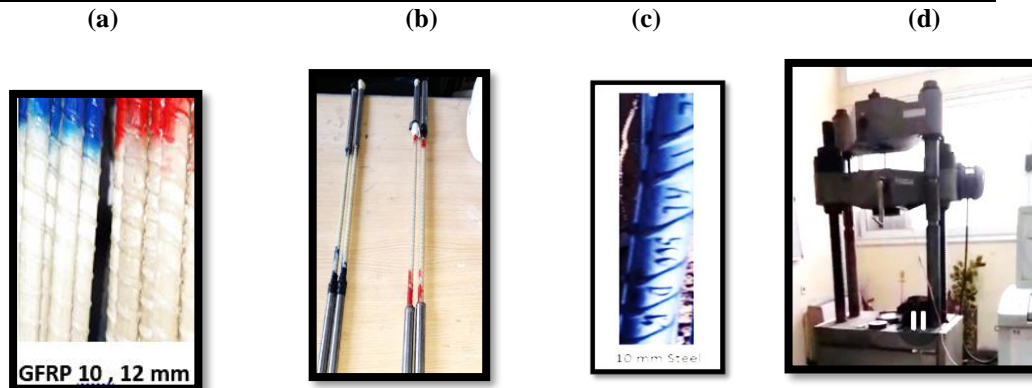


Fig. 6: (a) Samples of GFRP fiber bars; (b) preparing samples of GFRP; (c) steel bars; and (d) testing of tensile strength

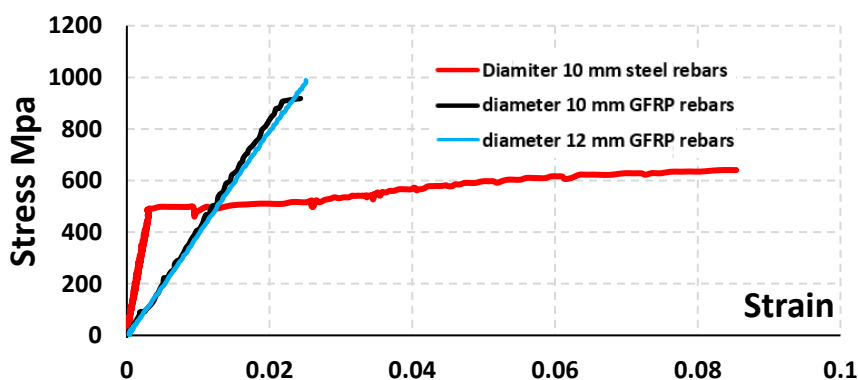


Fig. 7: Stress-Strain Curve for 10mm, 12mm steel, and GFRP Rebars

Table 4: Compressive strength for concrete mixes

Concrete mixes	Average ultimate compressive stress ( $f_c$ ) (MPa)		
	7 days (MPa)	28 days (MPa)	% of NMC
NC (0%)	34.70	40.0	100%
RBC (7.5%) (C.R.)	29.30	35.0	87.5%

**4. Methodology.**

The results of the control specimens BS, BS1, BH1, and BH2 with 0% C.R. were compared to those of the rubberized concrete beams BRF, BRH1, BRH2, and BRH3 with 7.5% C.R. under a static load test to check their flexure capacity and ductility index. Finally, the results were analyzed and discussed.

**5. Material and specimens**

**5.1 Materials**

Control mixes of normal concrete NC with a compressive strength of 40 MPa and a rubberized concrete RC of 35 MPa have been used. The NC mix used ordinary Portland cement with a relative density of 3.15, a water-to-cement ratio of 0.43, potable water, and natural crushed stone coarse

aggregates with a maximum size of 10 and 20 mm and a relative density of 2.57 g./cm<sup>3</sup>. For the RC mix, crumb rubber replaced sand by 7.5% by volume. A superplasticizer (Sikament R-2004) was used with a density of 1200 kg/m<sup>3</sup> (at 20 °C ASTM C 494/C494M-19e1) [33] to reduce water and enhance workability, as listed in Table 2. The aggregate sieve analysis satisfies the main grade Gc 90/15 and the additional grade G25/15 limits according to EN12620-2013 [34], as shown in Fig. 5. The mechanical properties of the used reinforcement have been defined using a 1000 kN capacity testing machine, as shown in Figs. 6 and 7. The GFRP bars have 10 and 12mm diameters and a tensile strength of 910 and 989 MPa, respectively. The steel bars had an average yield stress and tensile strength of 540 MPa and 641 MPa, respectively, as listed in Table 3. The average concrete compressive strength of the used mixes is listed in Table 4.

**5.2 Sample Preparation**

Eight full-scale beams with dimensions of 200 x 300 mm, a span of 1900 mm, and a flange width of 540 mm were used in this study. Mixing was performed by using a concrete-tilting drum mixer for five minutes. Concrete was placed and compacted mechanically by an internal electrical vibrator. After 24 hours, curing was applied for 7 days. The sample casting steps and preparation are shown in Fig. 8.

**5.3 Test setup and instrumentation**

The beam test-rig setup is shown in Fig. 9. A rigid steel spreader beam was used to spread the loads from the 5000 kN hydraulic jack to the loading plates. One strain gauge was attached longitudinally to the reinforcement bar at the center of the specimens. The loads were applied to the specimens by a 5000 kN capacity testing machine. The load was measured by the load cell, and the deformations and strains were recorded using LVDTs and strain gauges, respectively, as shown in Fig. 9.

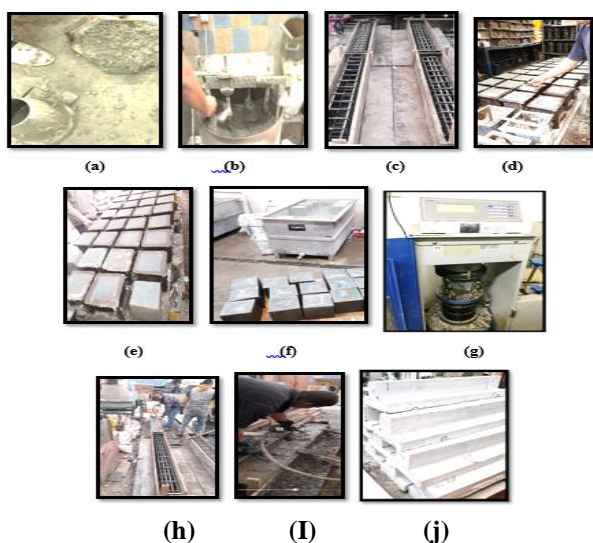


Fig. 8: Specimen preparation: (a) mixing of concrete; (b) slump test; (c) steel reinforcement; (d) preparing of cubs; (e) titling the cubs; (f) curing; (g) testing; (h) casting the concrete; (i) finishing; (j) all finished T-section beams

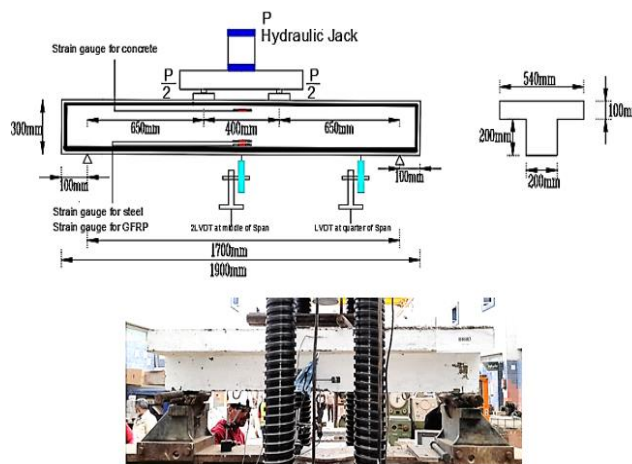


Fig. 9: Test setup schematic diagram

**6.Experimental results**

Sample BS had an ultimate load of 123.00 kN. The deflection corresponding to the ultimate load was 33.20 mm, and the mode of failure was considered to be a flexural failure. Sample BS1 had an ultimate load of 230.23 kN; the deflection corresponding to the ultimate load was 40.62mm; and a flexural mode of failure was encountered in this case as well. For beam sample BRF, the ultimate load was 149.34 kN, and the maximum deflection was 35.09 mm. The sample exhibited a combination of flexural and shear failures, followed by splitting modes of failure for GFRP bars. Sample BH1 had an ultimate load of 268.57 kN, and a deflection of 50.42mm with a flexural mode of failure. Beam sample BRH1 had an ultimate load of 237.19 kN, a maximum deflection of 52.77 mm, and a flexural mode of failure. The sample BH2 had an ultimate load of 269.83 kN, and a maximum deflection at the ultimate load of 52.39 mm, and the beam also exhibited a flexural mode of failure. For sample BRH2, the ultimate load has been recorded at 234.68 kN, a deflection of 57.67 mm, and a combination of flexural and shear failure with splitting for the GFRP bars. The last sample, BRH3, had an ultimate load of 248.49 kN and a maximum deflection of 29.79 mm. The mode of failure was a combination of shear failure and compression failure. The recorded experimental results in terms of first crack, yielding loads, and ultimate loads, as well as their corresponding deflections, are listed in Table 5 and Fig. 10. The load-displacement relation for all beams is shown in Fig. 11. The crack pattern at failure with the corresponding ultimate loads is listed in Table 6 and Fig. 13. The first crack deflection, yield deflection, and ultimate deflection of test specimens are shown in Fig. 12.

Table 5: Experimental results at first crack, yield load, and ultimate loads

Beam Model	Cracking Point		Yielding Point		Ultimate(peak) Point	
	$P_{cr}$ (kN)	$\Delta_{cr}$ (mm)	$P_y$ (kN)	$\Delta_y$ (mm)	$P_u$ (kN)	$\Delta_u$ (mm)
BS	42.67	0.418	65.26	2.16	123.00	33.20
BRF	27.61	0.345	40.16	4.85	149.34	35.09
BS1	43.42	0.49	75.22	3.45	230.23	40.62
BH1	44.18	0.69	101.65	5.97	268.57	50.42
BRH1	50.02	1.01	82.83	3.92	237.19	52.77
BH2	47.69	0.70	104.16	6.03	269.83	52.39
BRH2	55.22	1.59	110.44	4.66	234.68	57.67
BRH3	57.47	1.73	114.21	5.56	248.49	29.79

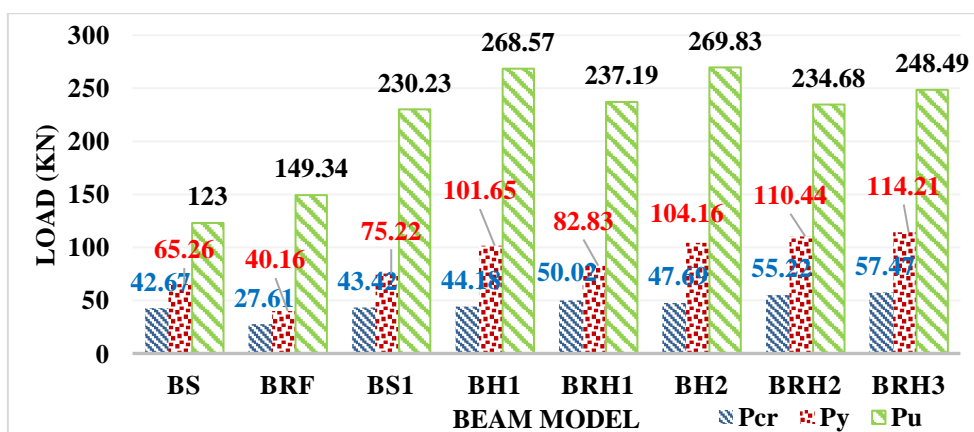


Fig. 10: First crack load, yield load, and ultimate loads of test specimens

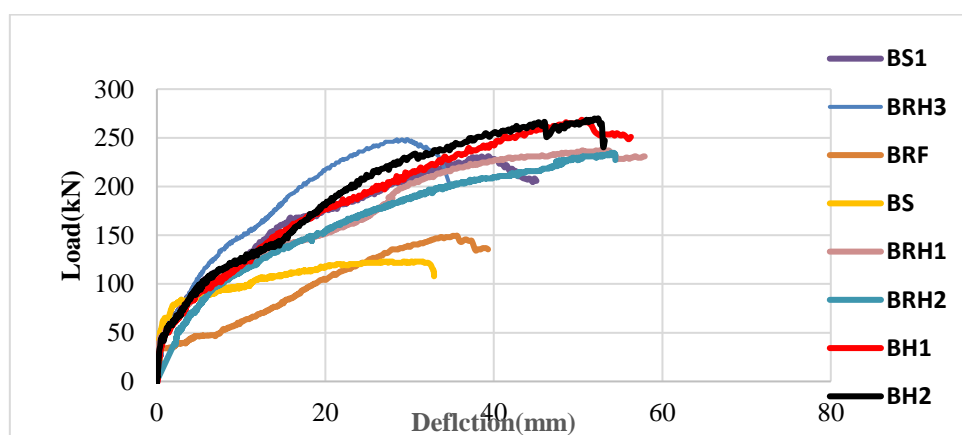


Fig. 11: Experimental load-deflection curve at mid-span

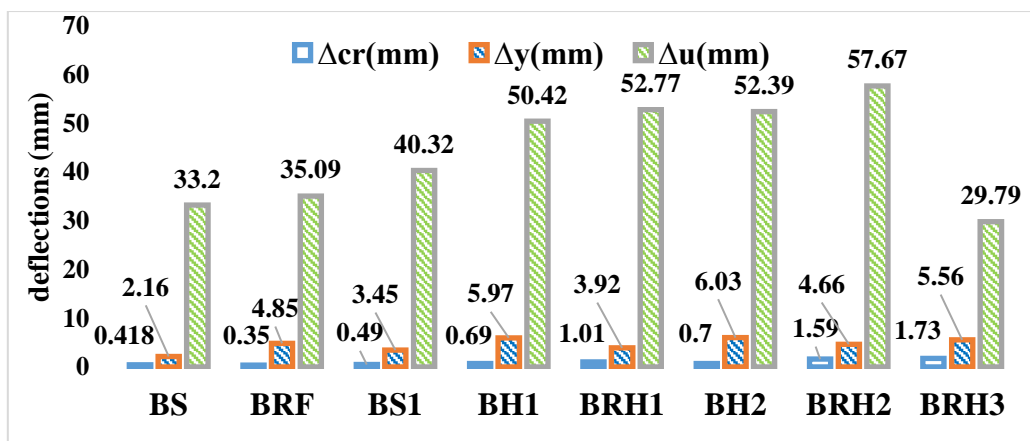










Fig. 12: Deflections at first, yield, and ultimate loads

Table 6: Experimental results of cracking load, yield load, ultimate load capacity, and mode of failure

Beam model	First crack load $P_{cr}$ (kN)	Yield Load $L_y$ (kN)	Ultimate load $L_u$ (kN)	Failure mode	Crack patterns of failure for the beams
BS	42.67	65.26	123.00	Flexural failure	
BRF	27.61	40.16	149.34	Combination of flexural and shear failure with splitting mode	
BS1	43.42	75.22	235.23	Combination of flexural and shear failure	
BH1	44.18	101.65	268.57	Flexural failure	
BRH1	50.02	82.83	237.19	Flexural failure	
BH2	47.69	104.16	269.83	Flexural failure	
BRH2	55.22	110.44	234.68	Combination of flexural and shear failure with splitting mode	
BRH3	65.26	114.21	248.49	Combination of shear failure and compression failure	



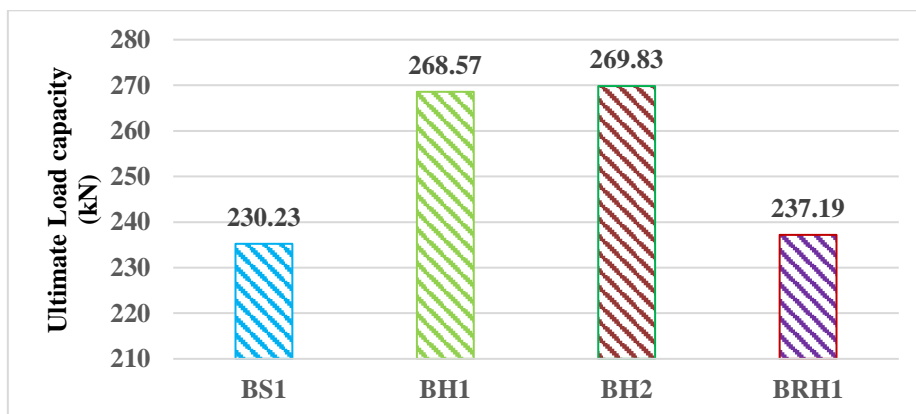


Fig.13: Load capacity for beams BS1, BH1, BH1, and BRH1

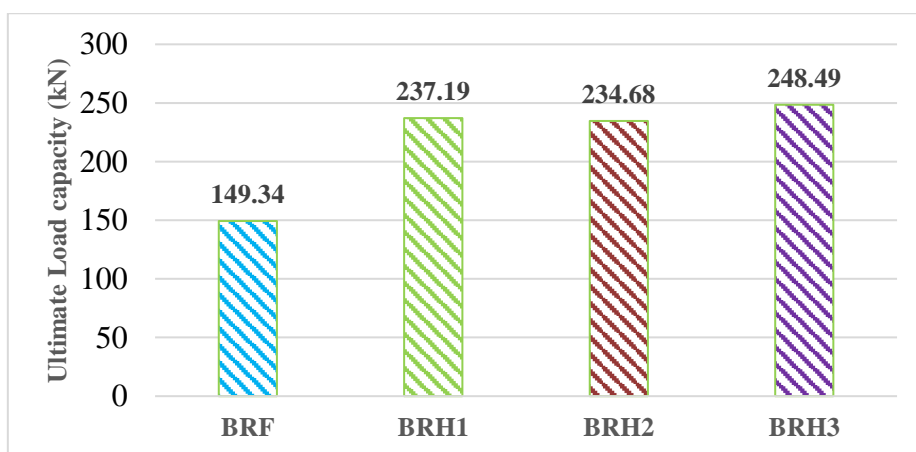


Fig. 14: Load capacity for beams BRF, BRH1, BRH2, and BRH3

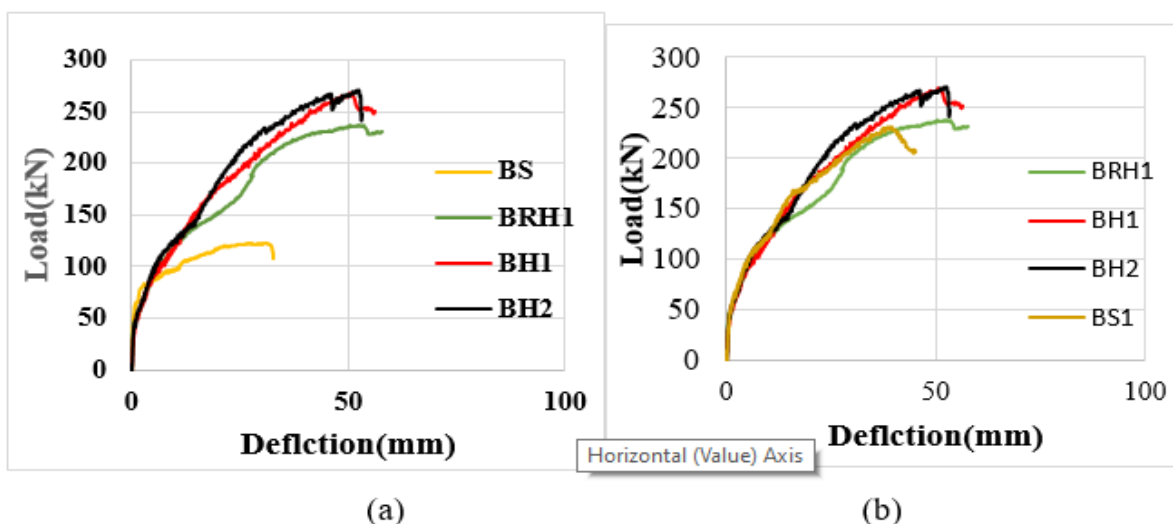


Fig. 15: Comparisons of load-displacement curves for beam samples

**Table 7: Ductility index for beam samples**

Beam Model	Ductility index - $\mu u = \Delta u / \Delta y$
BS	8.93
BRF	1.72
BS1	5.12
BH1	2.41
BRH1	4.32
BH2	2.70
BRH2	2.76
BRH3	1.15

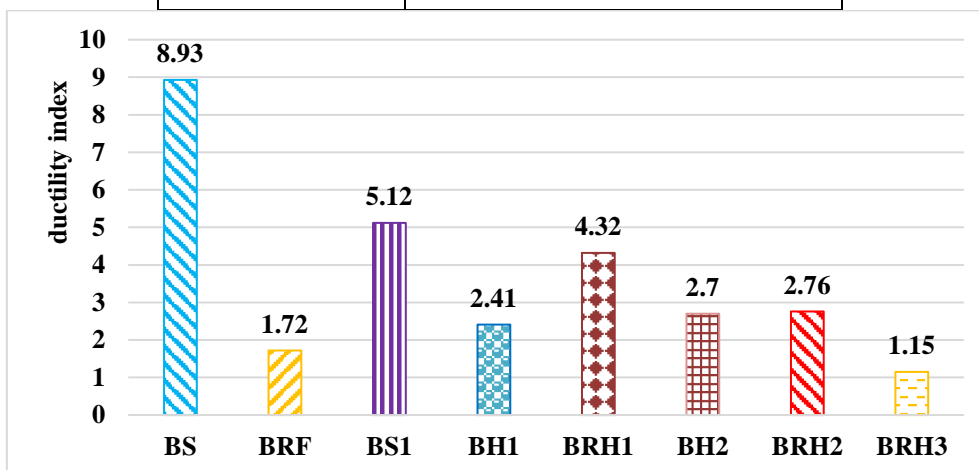


Fig. 16: Ductility index for beam samples

**Table 8: Energy dissipation for test specimens**

Beam Model	Energy dissipation $E_d$ (kN.mm)
BS	3162.5
BRF	3062.5
BS1	6300
BH1	10015
BRH1	9225
BH2	10340
BRH2	8838
BRH3	5450

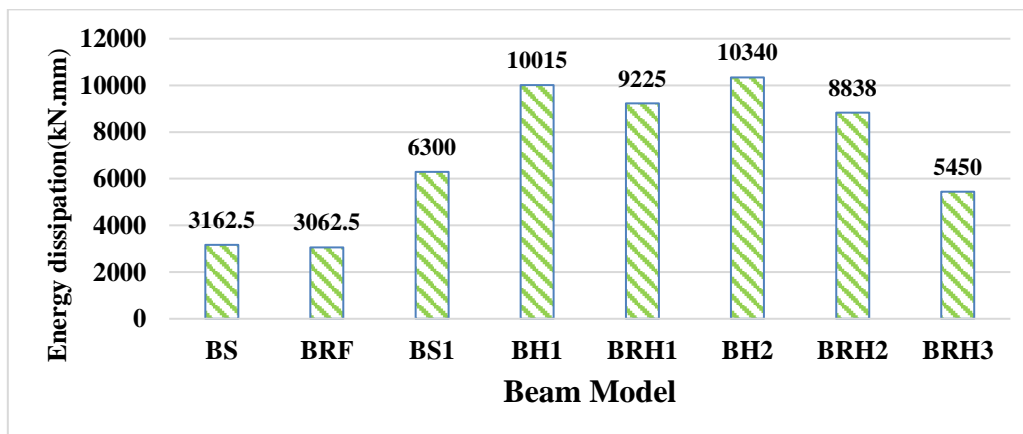


Fig. 17: Energy dissipation for test specimens

The hybrid-rubberized T-beams BRH1 and BRH2 decreased by 11.6% and 13%, respectively, compared to beams BH1 and BH2, which is attributed to the existence of rubber crumbs in the concrete matrix. The load capacity for hybrid rubberized beams BRH3 with 7.5% C.R. increased by 5.8% compared to the hybrid-rubberized T-beam BRH2, as shown in Fig. 14.

## 7.2 Deflection

The deflections increased for the hybrid beams BH1 and BH2 compared to BS1 (pure steel) by 30% and 35%, respectively, as shown in Fig. 15.b.

## 7.3 Ductility Index

The ductility of the structure refers to the deformation capacity; from the start of yielding to the maximum bearing capacity, or when the yield is not significantly determined, 80% to 85% of the peak load is considered. It is rather disadvantageous to use the displacement ductility factor because the yield deflection ( $\Delta_y$ ) is difficult to theoretically assess [30]. The ductility index is shown in Table 7 and Fig. 16. The maximum ductility index recorded was 8.93 for BS, and the minimum was 1.15 for BRH3.

The ductility index for hybrid T-beams BH1 and BH2 was lower than BS1 (pure steel) by 52.92% and 47.26%, respectively, as shown in Fig. 16, indicating that the ductility index of the hybrid T RC beams decreased compared to pure steel. In addition, the ductility index for the hybrid T-beam (BRH1) was lower than that of BS1 by 15.62%, indicating that the hybrid-rubberized RC T-beam BRH1 increased the ductility index compared to hybrid RC T-beams BH1 and BH2. The ductility index of hybrid rubberized T-beams (BRH1) increased by 79% compared to beam (BH1), as shown in Fig. 16, indicating that the rubberized hybrid RC-T-beam BRH1 increased the ductility index compared to the hybrid RC-T-beam BH1.

The ductility index for hybrid rubberized beams BRH3 (7.5% C.R.) decreased by 52.28% compared to the hybrid-rubberized T-beam BRH2 (7.5% C.R.). Hybrid-reinforced beam BRH3 has a ratio ( $A_f/A_s$ ) of 2.89.

## 7.4 Energy Dissipation

The energy absorption of beams is a good criterion for calculating the energy dissipation of the tested beams because the energy dissipation is the area within the load-unload curve. The energy absorption capacity is the area beneath the load-displacement curve under the assumption of reaching the failure load. The energy absorption of the samples was recorded based on the area below their load-displacement diagrams, up to 85% of the ultimate strength [27]. The energy dissipation of all samples has been calculated and listed in

Table 8 and Fig. 17. The lowest energy dissipation was recorded in sample BRF. The highest energy dissipation for hybrid samples was BH2, while the highest energy dissipation for hybrid-rubberized samples was BRH1.

Energy dissipation increased for hybrid T-beams BH1 and BH2 by 58.96% and 64.13%, respectively, compared to BS1. The hybrid-rubberized T-beams BRH1 increased their energy dissipation by 46.43% compared to BS1.

Energy dissipation increased for hybrid reinforcement T-beams BRH1 and BRH2 by 201% and 188.58%, respectively, compared to BRF (pure GFRP). This states that the rubberized hybrid reinforcement increases energy dissipation compared to pure GFRP reinforcement.

## 8. Conclusion

Hybrid beams with rubberized concrete have better performance compared to RC beams in terms of failure patterns and the number of cracks. Hybrid-RC beams combine the advantages of both classical steel reinforcement, which gives ductility, and the high ultimate strength provided by FRP reinforcement. In addition, the cost of GFRP reinforcement can be much lower than that of conventional steel reinforcement.

The following conclusions were obtained based on the achieved results:

1. The total load capacity for hybrid T-beams BH1 and BH2 with 0% crumb rubber (C.R.) was higher than that of T-beam BS1 with 0% C.R. by 16.65% and 17.2%, respectively, indicating that the load capacity of hybrid T-RC beams improved compared to pure steel.
2. Adding crumb rubber for hybrid T-beams BRH1 and BRH2 decreased the load capacity by 13.2% and 14.97%, respectively, compared to hybrid T-beams BH1 and BH2 with 0% C.R., indicating that the crump rubber decreased the total flexural capacity of the RC T-beam.
3. The deflection at the mid-span increased for the hybrid RC T-beams BH1 and BH2 by 30% and 35%, respectively, compared to BS1 (pure steel). The deflection for the hybrid-rubberized beams BRH1 and BRH2 increased compared to BRF (pure GFRP) by 111% and 94.4%, respectively.
4. The ductility index for hybrid T beams BH1 and BH2 was lower than beam BS1 (pure steel) by 52.92% and 47.26%, respectively, indicating that the ductility index of hybrid-T RC beams decreased compared to pure steel. In addition, the ductility index for hybrid-rubberized T-beams (BRH1) was lower than beam BS1 (pure steel) by 15.62%, indicating that the hybrid-rubberized T-beam BRH1 increased the ductility index compared to hybrid T-beam BH1, BH2.

5. The ductility index for hybrid-rubberized beams BRH1 and BRH2 increased by 74.41% and 60.46%, respectively, compared to T-beam BRF (pure GFRP), preventing the brittle failure of GFRP RC-T beams. Adding steel reinforcement to GFRP RC-T beams increased the ductility index for hybrid-rubberized beams BRH1 and BRH2 compared to the beam BRF (pure GFRP).
6. The ductility index for hybrid-rubberized T-beams (BRH1) increased by 28.2% compared to BH1, indicating that the hybrid-rubberized T-beam BRH1 increased the ductility index compared to the hybrid T-beam BH1.
7. Energy dissipation increased for hybrid T-beams BH1 and BH2 by 58.96% and 64.13%, respectively, compared to BS1. The hybrid-rubberized T-beams BRH1 increased their energy dissipation by 46.43% compared to BS1. This states that the rubberized hybrid T-beam increases energy dissipation compared to pure steel.

#### Declaration of interests

The authors declare that they have no known competing financial interests or personal relationships that could have appeared to influence the work reported in this paper.

#### Data availability statement (DAS)

The data sets generated during and/or analyzed during the current study are available from the corresponding author upon reasonable request.

#### References

- [1] A.F. Ashour, Flexural and shear capacities of concrete beams reinforced with GFRP bars, *Constr. Build. Mater.* 20 (2006) 1005-1015.
- [2] B. Benmokrane, O. Chaallal, and R. Masmoudi, Flexural response of concrete beams reinforced with FRP reinforcing bars, *Case Studies in Construction Materials* 14 (2021) e00513-16.
- [3] P.H. Bischoff, Deflection calculation of FRP-reinforced concrete beams based on modifications to the existing Branson equation, *J. Compos. Constr.* 11 (2007), 4–14.
- [4] .F. Kara and A.F. Ashour, Flexure design methodology for concrete beams reinforced with fiber-reinforced polymers, *Compos. Struct.* 94 (2012) 1616–1625.
- [5] H.A. Rasheed, I.R. Naye, and H. Melhem, Response prediction of concrete beams reinforced with FRP bars, *Compos. Struct.* 65 (2004) 193–204.
- [6] A.G. Razaqpur, D. Svecova, and M.S. Cheung, Rational method for calculating the deflection of fiber-reinforced polymer-reinforced beams, *ACI Struct. J.* 97 (2000), 175–184.
- [7] H. Toutanji and Y. Deng, Deflection and crack-width prediction of concrete beams reinforced with glass FRP rods, *Constr. Build. Mater.* 17 (2003), 69–74.
- [8] H. Toutanji and M. Saafi, Flexure behavior of concrete beams reinforced with glass fiber-reinforced polymer (GFRP) bars, *ACI Struct. J.* 97 (2000), 712–719.
- [9] P.V. Vijay and H.V.V. Gangarao, bending behavior and deformability of glass fiber-reinforced polymer-reinforced concrete members, *ACI Struct. J.* 98 (2001), 834–842.
- [10] J.R. Yost, S.P. Gross, Flexure design methodology for concrete beams reinforced with fiber-reinforced polymers, *ACI Struct. J.* 99 (2002), 308–316.
- [11] H. Böhni, editor, *Corrosion in reinforced concrete structures*. Woodhead Publishing Limited (2005).
- [12] B. Benmokrane, O. Chaallal, and R. Masmoudi, Glass fiber reinforced plastic (GFRP) rebars for concrete structures, *Construction and Building Materials*, Volume 9, Issue 6, (1995), pp. 353-364.
- [13] M. N. Habeeb and A. F. Ashour, Flexural behavior of continuous GFRP-reinforced concrete beams. *J Compos. Constr.* (2008) 12(2):115–24.
- [14] M. E. M. Mahroug, A.F. Ashour, and D. Lam, Tests of continuous concrete slabs reinforced with carbon fiber-reinforced polymer bars. *Compos. B* (2014),66:348–57.
- [15] H. Wang and A. Belarbi, Ductility characteristics of fiber-reinforced concrete beams reinforced with FRP rebars. *Construction Build Materials* (2011);25(5):2391–401.
- [16] M. M. Hasona, M. H. Mussab, and A.M. Abdulhadib, Flexural ductility performance of hybrid-recycled aggregate reinforced concrete T-beam, *Materials Today*, Volume 46, Part 1, (2021), Pages 682-688.
- [17] Yang Y, Sun ZY, Wu G., Cao DF, and Pan D. Experimental study of concrete beams reinforced with hybrid bars (SFCBs and BFRP bars). *Material and Structures*, 53, 77 (2020). <https://doi.org/10.1617/s11527-020-01514-8>.
- [18] Kocaoz S., Samaranyake VA, and Nanni A. Tensile characterization of glass FRP bars. *Composites: Part B: Engineering*, 36, pp. 127–34, 2005.
- [19] A. Si Larbi, E. Ferrier, and H. Patrice, Flexural behavior of MRBC beams (multi-reinforcing bars concrete beams), promoting the use of FRHPC. *Compos. Struct.* (2006); 74(2):163–74.
- [20] W. Qu, X. Zhang, and H. Huang, Flexural Behavior of Concrete Beams Reinforced with Hybrid (GFRP and Steel) Bars. *J Compos. Constr.* (2009); 13(5):350–9.
- [21] D. Laua and H. J. Pam, Experimental study of hybrid FRP-reinforced concrete beams. *Eng Struct* (2010); 32(12):3857–65.
- [22] Y. S. Yoon, J. M. Yang, K. H. Min, H. Oh, Shin, Flexural strength and deflection characteristics of high-strength concrete beams with hybrid FRP and steel bar reinforcement. 10<sup>th</sup> International Symposium on Fiber-Reinforced Polymer Reinforcement for Concrete Structures (2011), FRPRCS-10, in conjunction with the ACI Spring 2011.
- [23] L. Pang, W. Qu, P. Zhu, and J. Xu, Design propositions for hybrid FRP-steel-reinforced concrete beams. *Composite Construction* 2016; 20(4):04015086.
- [24] M.F.M. Fahmy, L.K. Idriss, Flexural behavior of large-scale semi-precast reinforced concrete T-beams made of natural and recycled aggregate concrete, *Eng. Struct.* 198 (2019) 109525, <https://doi.org/10.1016/j.engstruct.2019.109525>.
- [25] A. Younis, U. Ebead, and S. Judd' Life cycle cost analysis of structural concrete using seawater, recycled concrete aggregate, and GFRP reinforcement,
- [26] H. Almahmood, A. Ashour, and T. Sheehan, Flexural behavior of hybrid steel-GFRP-reinforced concrete continuous T-beams, *Composite Structures*, 254 (2020), 112802.
- [27] S. Moolaei, M. K. Sharbatdar, and A. Kheyroddin, Experimental evaluation of flexural behavior of HPRCC beams reinforced with hybrid steel and GFRP bars, *Composite Structures*, 275 (2021), 114503.

- [28] M. Nematzadeh and S. F. Valukolae, Experimental and analytical investigation on the structural behavior of two-layer fiber-reinforced concrete beams reinforced with steel and GFRP rebars, *Constr. Build. Mater.* Volume 273, (2021), 121933.
- [29] L. Yinghao and Y. Yong, Arrangement of hybrid rebars on the flexural behavior of HSC beams. *Compos B Eng* (2013); 45(1):22–31.
- [30] Z. Sun, L. Fua, D. Feng, A. R. Vatuloka, Y. Wei, and G. Wu, Experimental study on the flexural behavior of concrete beams reinforced with bundled hybrid steel/FRP bars, *Engineering Structures*, 197 (2019), 109443.
- [31] M. K. Ismail, A. A. Hassan, Performance of Full-Scale Self-Consolidating Rubberized Concrete Beams in Flexure. *ACI Material Journal* (2015) 166.4
- [32] 440.1R-015, A. Guide for the Design and Construction of Structural Concrete Reinforced with Fiber Reinforced Polymer (FRP) Bars (ACI 440.1 R-15). American Concrete Institute, Farmington Hills, MI.
- [33] ASTM International, ASTM C 494/C494M-19e1, Standard Specification for Chemical Admixtures for Concrete, (2020).
- [34] British Standard, EN12620 aggregates for concrete ,(2013).